Available online at www.sciencedirect.com
ScienceDirect
Trans. Nonferrous Met. Soc. China 33(2023) 1540−1549
Transactions of Nonferrous Metals Society of China
www.tnmsc.cn

Preparation and electrocatalytic hydrogen evolution performance of spherical hollow MoS_2/WS_2 heterostructures

De-zhi WANG, Liu-yi-yi YANG, Ruo-qi LIU, Ting GUO, Hao FEI, Zhuang-zhi WU

School of Materials Science and Engineering, Central South University, Changsha 410083, China

Received 26 November 2021; accepted 30 March 2022

Abstract: A heterostructure composed of spherical hollow WS_2 and petal-like MoS_2 was systematically studied. The results showed that the spherical hollow structures exposed more active sites, and the construction of heterostructures triggered the synergistic effect between WS_2 and MoS_2 and improved the hydrogen evolution reaction (HER) performances with better electron transfer ability. More importantly, the density functional theory calculations further clarified the synergistic mechanism, in which the MoS_2/WS_2 heterostructure could effectively regulate the hydrogen adsorption free energy to achieve the minimum value with a W/Mo atomic ratio of 2:25. Consequently, the optimized WMo-2/25 catalyst exhibited superior electrocatalytic HER activity with a low Tafel slope of 53 mV/dec as well as good durability.

Key words: molybdenum disulfide; tungsten disulfide; heterostructures; hydrogen evolution reaction; density functional theory

1 Introduction

With the development of human society, the energy demand has significantly increased. As the dominant energy, the consumption of traditional fossil fuels is rapidly increasing, and their limited reserves are bound to constrain significant use in the long term. In addition, the consumption of fossil fuel produces a large number of harmful substances, leading to serious problems of environmental pollution and deterioration of the ecological environment around the earth. Therefore, the development and application of sustainable clean energy become important and urgent [1−3]. As a green and pollution-free clean energy [4], hydrogen has a broad prospect in application with the advantages of abundant reserves, high combustion value, and is not constrained by region and natural environment [5]. Replacing conventional energy sources with hydrogen energy is a desirable goal that has received plenty of attention. Hydrogen can be prepared in three main ways. The first one is the production of hydrogen from fossil fuels [6], but it is contrary to the ultimate goal of environmental protection. The second one is the use of bioenergy [7]. However, this method cannot be achieved through large-scale industrial production due to immature technology. The third one is water splitting through sustainable electrochemical processes such as photoelectrocatalysis or electrolysis driven by an external renewable source of electricity [8]. Limited by high cost and low reserves, although Pt-based compounds are considered to be the most efficient electrocatalysts for hydrogen evolution reaction (HER) [9], they cannot achieve sustainable and large-scale applications. Therefore, the search for efficient and cheap catalysts to replace noble metals has attracted increasing attention [10−13].

As an effective catalyst for HER, transition metal sulfides have been widely reported, including

Corresponding author: Zhuang-zhi WU, Tel: +86-13974889625, E-mail: zwu@csu.edu.cn
DOI: 10.1016/S1003-6326(23)66201-6

molybdenum sulfide (MoS_2) [14,15], tungsten sulfide (WS_2) [16−18], nickel sulfide (NiS_2) [19,20], and cobalt sulfide (CoS_2) [21,22], etc. Among them, MoS_2 and WS_2 have gradually become the alternatives to noble metal catalysts owing to their high activities. A large number of reports have shown that the catalytic activities of MoS_2 and WS_2 can be improved by providing more active sites [23], increasing specific surface area [24], enhancing electron transfer ability [25−27], and constructing heterostructures [25,28,29]. CHEN et al [23] compared the HER performance of MoS_2 and WS_2; however, there was little explanation about their synergistic effect. KIM et al [16] achieved improved catalyst performance by growing MoS_2 and WS_2 on nickel foam coated with reduced graphene oxide (rGO). Nevertheless, it is difficult to control the uniformity of materials adhesion, and nickel foam is not suitable for acidic electrolytes. Therefore, it is an interesting challenge to prepare MoS_2/WS_2 catalyst with excellent performance and suitable for acidic conditions by simplifying the experimental process.

In this work, we proposed unique MoS_2/WS_2 heterostructures prepared by a combination of high-temperature calcination and hydrothermal method, in which WS_2 with a spherical shell structure expands the specific surface area, and MoS_2 with a thin edge provides more active sites for the HER. Moreover, by adjusting the atomic ratio of W to Mo, we regulated the microstructures and obtained the best catalytic performances with a Tafel slope of 53 mV/dec and good stability in acidic conditions.

2 Experimental

2.1 Synthesis of silica templates

Typically, 7 mL tetraethyl orthosilicate (TEOS) was put dropwise to a homogeneous solution mixed with 92 mL ethanol, 17.2 mL deionized water, and 5 mL ammonia. The obtained mixture was stirred at room temperature for 3 h. The collected precipitates were washed with deionized water and ethanol thrice, and then dried at 80 °C for 12 h. Finally, the silica templates can be obtained.

2.2 Synthesis of spherical hollow WS_2 (p-WS_2)

1 mmol WO_3, 6 mmol NH_2CSNH_2 and 10 mmol silica templates were dispersed in 25 mL ethanol and then sonicated for 30 min. After drying, the pale-yellow mixture powder was fully ground with 2 mmol Na_2SO_3. In the atmosphere of argon, the powder mixture was calcined at 200 ℃ for 3 h, and then calcined at 600 ℃ for 3 h. The calcined powder was put into hydroxide sodium solution to remove templates and unreacted substances, washed and then dried overnight at 80 ℃.

2.3 Synthesis of catalysts

The MoS_2/WS_2 catalysts were synthesized by a facile hydrothermal method. 0.4 mmol p-WS_2, 5 mmol $Na_2MoO_4{\cdot}2H_2O$ and 5 mmol $C_5H_{10}NNaS_2{\cdot}3H_2O$ were added in a mixture of 30 mL ethanol and 30 mL deionized water, and stirred for 30 min. Next, the mixture was transferred to a reactor and placed in the oven at 180 °C for 12 h. And the as-prepared product was named as WMo-2/25.

Catalysts with various atomic ratios of W to Mo were also obtained following the same procedure by changing the amount of molybdenum source (2 and 10 mmol), and the corresponding products were named as WMo-5/25 and WMo-1/25, respectively. Additionally, pure MoS_2 (named as srMoS_2) was also synthesized by the same procedure in the absence of WS_2.

All the detailed information of reagents and materials can be found in the Supporting information (SI).

2.4 Characterization

The X-ray diffraction patterns (XRD) were obtained by an X-ray diffractometer (Rigaku D/Max 2500, with a diffraction source of Cu K_α). The microstructures were captured by MIRA4 LMH scanning electron microscope (SEM) and Titan G260−300 transmission electron microscope (TEM/HRTEM). The surface element analysis was performed by Ultim Max 40 X-ray spectrometer (EDS). X-ray photoelectron spectroscopy (XPS) was detected on the Thermo Scientific photoelectron spectrometer.

2.5 Electrochemical tests

The electrochemical hydrogen evolution performances were evaluated on the electro-chemical workstation (CHI660E, Shanghai Chenhua, China) in 0.5 mol/L H_2SO_4 with saturated calomel electrode, carbon rod, and glassy carbon electrode loaded with catalysts as the reference,

counter, and working electrodes, respectively.

Typically, 3 mg of catalyst, 80 μL of Nafion solution (5 wt.%, Du Pont), and 200 μL of ethanol were put into 800 μL of deionized water to form a homogeneous ink. Then, 5 μL of the slurry was loaded on the surface of the working electrode, and then naturally dried.

The polarization curves were obtained by the linear scanning voltammetry (LSV) with a scanning speed of 2 mV/s, and the electrochemical impedance spectroscopy (EIS) was measured from to 1 MHz to 1 Hz at −150 mV. The stability curves were obtained from 1000 continuous cyclic voltammetry scans and 10 h of constant voltage *I*–*t* tests. And the Tafel slope was calculated following Eq. (S1) in the Tafel formula of SI.

3 Results and discussion

3.1 Microstructure of sample

Figure 1 shows the XRD patterns of various samples, in which $srMoS_2$ displays a similar peak distribution to MoS_2 (JCPDS No.75-1539), but the (002)' diffraction peak shifts to 9.4°, indicating a larger inter-layer spacing. The (004)' peak is the second-order diffraction peak of (002)' [30], and the interplanar spacing calculated from (004)' peak is about 4.95 Å by the Bragg equation. In the diffraction pattern of p-WS_2, four obvious diffraction peaks are found, including the (002), (101), (103) and (110) reflections, and well matched with the standard WS_2 (JCPDS No.84-1398). Moreover, with the decreased W/Mo atomic ratio, the (002)' diffraction peak of MoS_2 is gradually enhanced.

Figure S1 in SI shows the Raman spectra, in which $srMoS_2$ displays the characteristic E^1_{2g} and A_{1g} (372.6, and 399.9 cm^{-1}) peaks [31,32] of MoS_2. In the WMo-2/25 spectrum, except the characteristic MoS_2 peaks, the E^1_{2g} and A_{1g} peaks (349 and 413.3 cm^{-1}) [33] of WS_2 can also be observed, further demonstrating the coexistence of WS_2 and MoS_2.

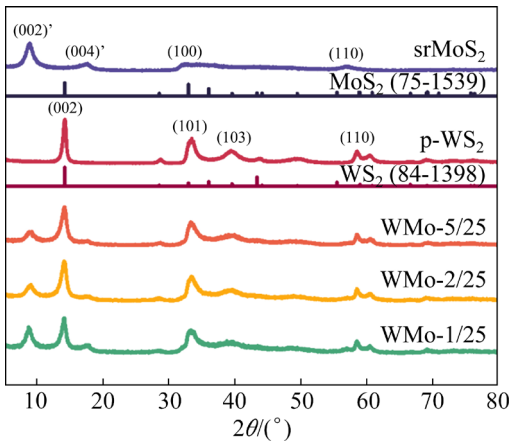

Fig. 1 XRD patterns of various samples

Figure 2 shows the microstructures of various samples. In Fig. 2(a), $srMoS_2$ is large and irregular petals. In Fig. 2(b), p-WS_2 inherits the uniform spherical morphology of SiO_2 nanospheres (Fig. S2(a) in SI), and the corresponding diameter is slightly larger than that of hard templates. With a few Mo addition, both WMo-5/25 (Fig. S2(b) in SI) and WMo-2/25 (Fig. 2(c)) inherit the spherical hollow structures of p-WS_2 and petal structures of $srMoS_2$, which is beneficial to exposing more active sites. However, for WMo-1/25 (Fig. S2(c) in SI), MoS_2 adheres to WS_2 spherical shells and agglomerates seriously. The EDS mappings (Figs. 2(d_2–d_4)) of the WMo-2/25 demonstrate the well-dispersion of Mo, W and S elements in the catalyst.

By magnifying the petal structures of $srMoS_2$ (Fig. 3(a_1)), the interlayer spacing of $srMoS_2$ is about 4.9 Å (Fig. 3(a_2)). In WMo-2/25 (Fig. 3(b_1)), the petal-shaped $srMoS_2$ is closely bound to the spherical p-WS_2 shells, and two different spacings can be measured, including 6.2 Å and 4.9 Å, as depicted in Fig. 3(b_2). According to the XRD analysis results, the former belongs to the (002) crystal plane of WS_2, and the latter is the (004)' of MoS_2, further demonstrating the coexistence of WS_2 and MoS_2 in WMo-2/25.

According to the XPS survey spectrum of WMo-2/25 (Fig. 4(a)), there are W, Mo, S, C, O and N in the sample. And the W 4f spectrum (Fig. 4(b)) exhibits two peaks at 32.6 and 34.8 eV, corresponding to the W^{4+} states [34]. The peaks located at 36.1 and 38.2 eV can be attributed to W^{6+} species [35,36], resulting from inevitable oxidation on the surface. In Fig. 4(c), the double peaks at 228.4 and 231.5 eV can be assigned to Mo 3d of MoS_2, and the peaks appeared at 232.4 and 235.5 eV should be ascribed to MoO_3 [37]. Additionally, the peaks of S 2s and Mo^{3+} are observed at 225.6 and 228.9 eV [38,39], respectively. In the S 2p spectrum (Fig. 4(d)), the peaks at 161.2 and 162.3 eV are indexed to the binding energies of S^{2-} $2p_{3/2}$ and S^{2-} $2p_{1/2}$ [40], the

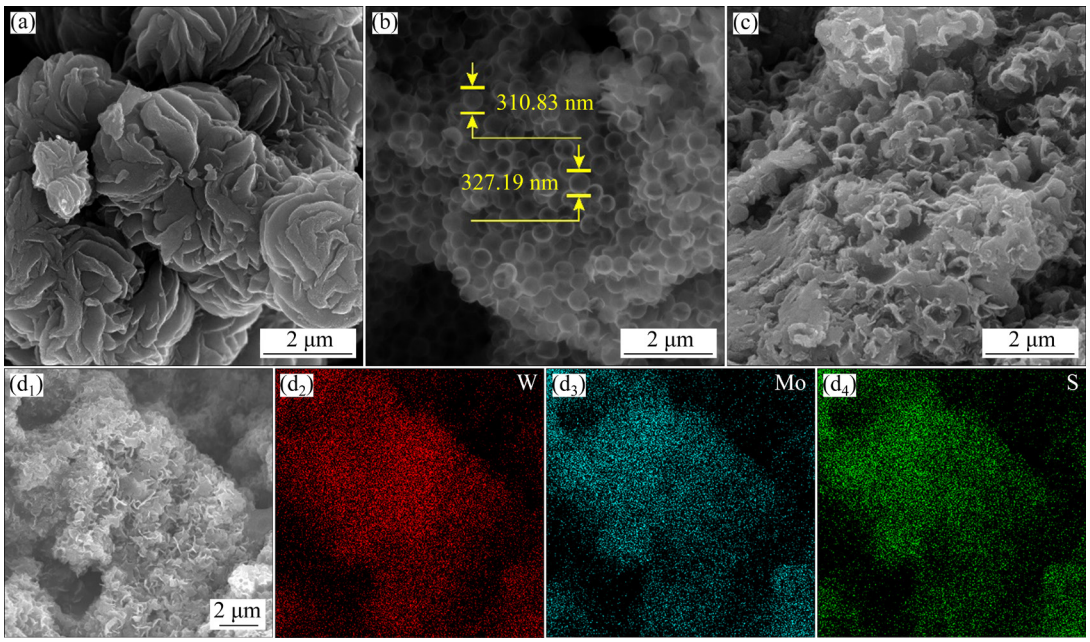

Fig. 2 SEM images of $srMoS_2$ (a), p-WS_2 (b) and WMo-2/25 (c, d_1), and corresponding EDS elemental mapping of WMo-2/25 (d_2−d_4)

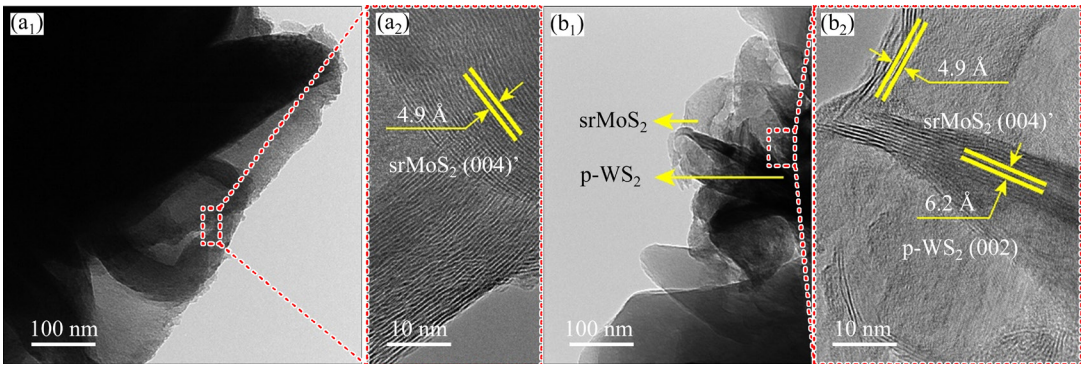

Fig. 3 TEM (a_1, b_1) and HRTEM (a_2, b_2) images of $srMoS_2$ (a_1, a_2), and WMo-2/25 (b_1, b_2)

peaks at 162.6 and 163.8 eV correspond to the binding energies of S_2^{2-} [41], and the peak at 168.48 eV belongs to sulfate groups [42]. Moreover, the presence of C and O can also be further revealed by Fig. S3 in SI.

3.2 Electrochemical performance

The HER performance of various samples was evaluated in a three-electrode system in 0.5 mol/L H_2SO_4 (Table 1). As shown in Fig. 5(a), the commercial Pt/C catalyst still exhibits the best electrocatalytic performance with the smallest Tafel slope of 30 mV/dec, consistent with the previous reports [36,43]. The WMo-2/25 catalyst also shows excellent HER performances compared with other counterparts with a small Tafel slope of 53 mV/dec (the Tafel formula, Eq. (S1) in SI), and only requires −280 mV to achieve 10 mA/cm^2, much better than other electrocatalysts with various W/Mo atomic ratios, as compared in Table 1.

Generally, the HER can be divided into two processes and three possible steps in acidic electrolyte [6]. The first one is the discharge process, in which electrons transferred to the electrode surface react with protons to generate adsorbed intermediate hydrogen atoms (H_{ads}) (Volmer reaction, Eq. (S2) in SI). And the other one is the desorption process, in which Heyrovsky reaction occurs at a low concentration of H_{ads} (Eq. (S3) in SI), while the Tafel reaction occurs under high concentration (Eq. (S4) in SI). Moreover, the corresponding Tafel slopes are 120, 40 and 30 mV/dec [6], respectively. Then, the corresponding HER mechanism and rate-controlling steps can be

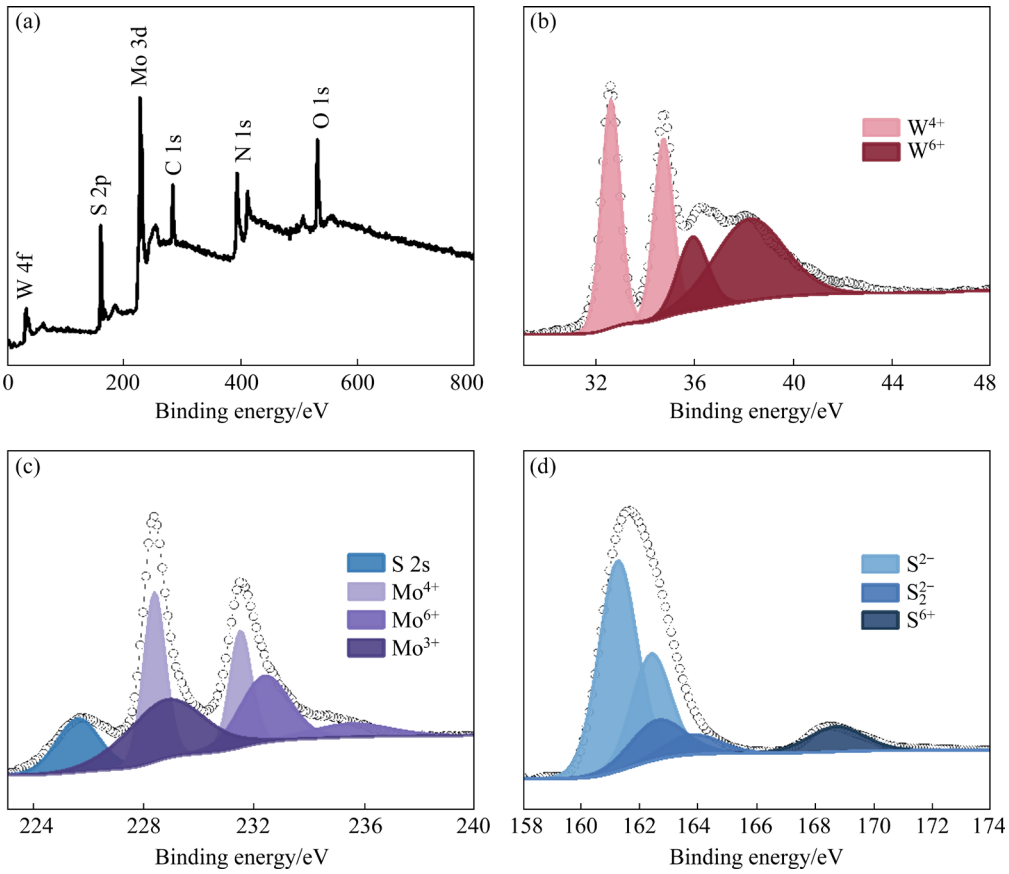

Fig. 4 XPS spectra of WMo-2/25: (a) Survey; (b) W 4f; (c) Mo 3d; (d) S 2p

Table 1 Electrocatalytic HER performance of various samples

Catalyst	Tafel slope/(mV·dec^{-1})	Overpotential, η/ mV	C_{dl}/(μF·cm^{-2})	A_{ECSA}/cm^2	R_{ct}/Ω
Pt/C	30	−20	–	–	–
p-WS_2	99	–	660	11	–
WMo-5/25	82	−340	4770	79.50	400
WMo-2/25	53	−280	4946	82.43	120
WMo-1/25	88	−360	2308	39.67	340
srMoS_2	119	–	1073	17.88	–

deduced [44]. The Tafel slope of WMo-2/25 (53 mV/dec) in this work is much smaller than that of other counterparts (Fig. 5(b)), implying a Volmer−Heyrovsky mechanism. It is worth noting that the Tafel slopes of all the composed catalysts are lower than those of p-WS_2 and srMoS_2, indicating that the construction of heterostructures is also one of the effective ways to improve the HER performance.

The electron transfer ability is also an important factor to evaluate the kinetics of HER catalysts [45]. The charge transfer impedance (R_{ct}) of various catalysts in the HER can be obtained by fitting the EIS with a suitable circuit model. As shown in Fig. 5(c), the R_{ct} of p-WS_2 and srMoS_2 is much larger than that of composed catalysts, and the R_{ct} of composed catalysts depends on the Mo addition, in which the R_{ct} of WMo-2/25 (120 Ω) is the minimum, indicating the strongest electron transfer ability.

Stability is another important indicator for applications of catalysts. As shown in Fig. 5(d), the WMo-2/25 could maintain the catalytic activity for 10 h without significant decrease, and the polarization curves only show slighter decay compared with the initial one after 1000 CV cycles (inset in Fig. 5(d)), demonstrating good stability under acidic conditions.

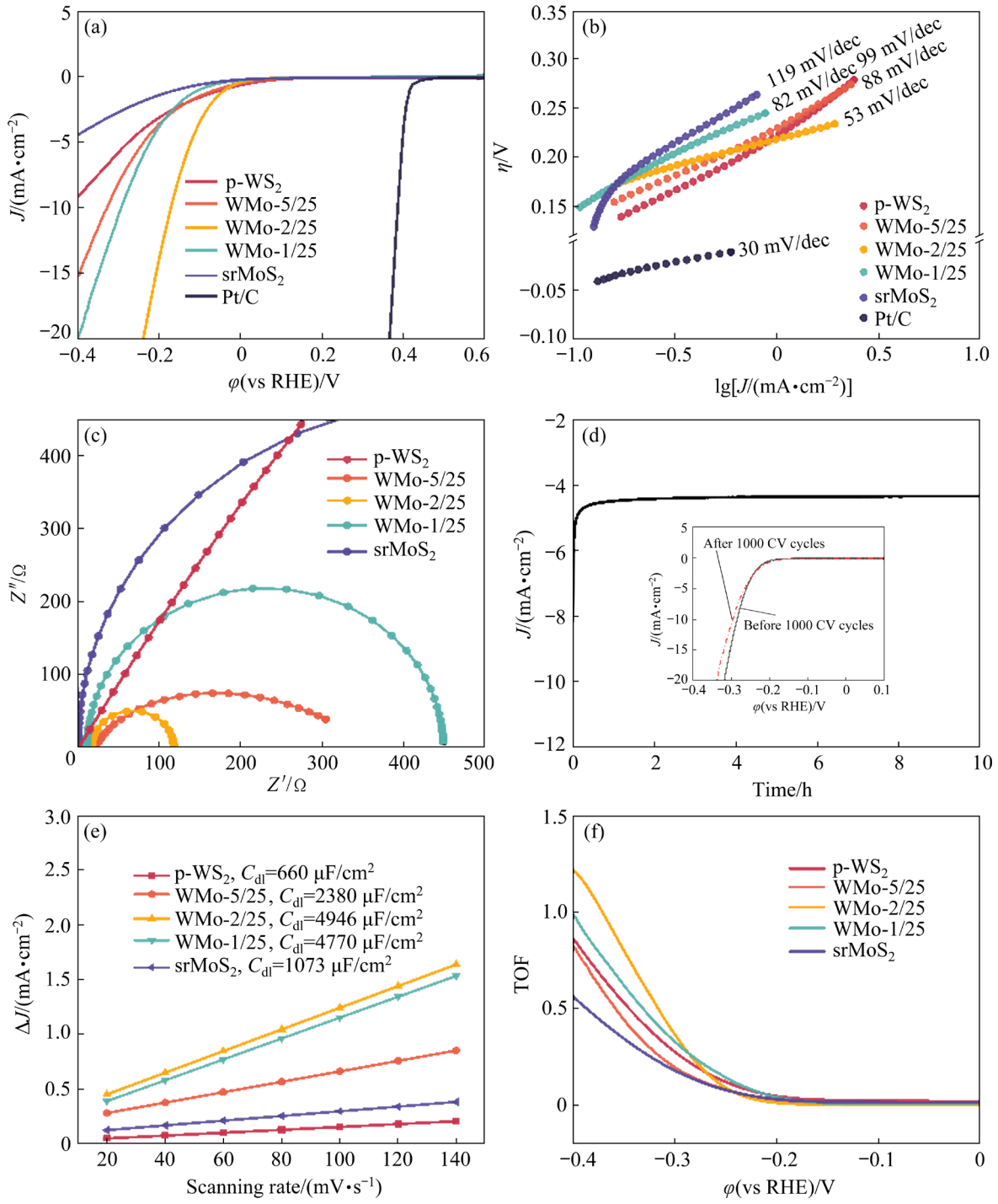

Fig. 5 Electrocatalytic HER performance of various samples in 0.5 mol/L H_2SO_4: (a) LSV polarization curves; (b) Tafel plots; (c) EIS at 250 mV vs RHE; (d) Chronoamperometry of WMo-2/25 at −0.2 V (Inset shows the polarization curves of WMo-2/25 before and after 1000 CV cycles); (e) Capacitive currents at 0.15 V (vs RHE) as function of scan rate; (f) TOF curves

The cyclic voltammetry (CV) curves of samples at different scanning rates (20, 40, 60, 80, 100, 120, and 140 mV/s) (Fig. S4 in SI) were measured in the voltage range without Faraday reaction. The curves (Fig. 5(e)) were drawn with scanning rates as the abscissa and the change of capacitance current value as the ordinate, and half of their linear slopes were the electrochemical double-layer capacitances (C_{dl}) [46−49]. Generally, the electrochemical active surface area (A_{ECSA})

can be considered to represent the number of active sites [50,51], and A_{ECSA} value of samples can be estimated by Eq. (S5) in SI. Obviously, the A_{ECSA} of WMo-2/25 (82.43 cm^2) is the maximum. The turnover frequency (TOF) represents the HER catalytic activity of each active site, and the corresponding curves (Fig. 5(f)) were converted from the polarization curve following Eq. (S6−S9) and Table S1 in SI. It can be observed that pure p-WS_2 exhibits the largest TOF value, and the TOF value is gradually reduced with the increased content of Mo. However, it should be noted that the variation is not significant, and the WMo-2/25 catalyst still possesses a comparable TOF value with that of p-WS_2.

Based on the above analysis, compared with those of p-WS_2 and srMoS_2, the enhanced HER activity of WMo-2/25 is believed to be a direct consequence of the formation of MoS_2/WS_2 heterostructures. With the decrease of W/Mo molar ratio, the formation of heterostructure is gradually increased, which is conducive to the enhancement of hydrogen evolution performance, and achieves the maximum at molar ratio of 2:25. Afterwards, the HER activity is gradually reduced with the decreased W/Mo molar ratio, because too much MoS_2 will aggregate and block the spherical shell structure of WS_2, resulting in a sharp reduction of the specific surface area as well as the exposed active sites.

3.3 DFT calculations

All spin-polarized density functional theory (DFT) calculations were performed via the Vienna ab initio Simulation Package (VASP) code. The exchange-correlation interactions were described by the Perdew-Burke-Enzerhof (PBE) pseudo-potentials of generalized gradient approximation (GGA), and the van der Waals interaction was calculated using the vdW-D3 method developed by Grimme. To get deep insights into the improvement mechanism, a model of WMo-2/25 is established (Fig. 6(a)), and the Gibbs free energy (ΔG_H) of each sample is obtained by DFT calculations (Fig. 6(b)) following Eqs. (S10) and (S11) in SI. In the HER process, the excessive adsorption or desorption capacity of hydrogen can hinder the catalytic ability and affect the smooth generation of H_2. Therefore, for an ideal electrocatalyst, the ΔG_H should be close to 0 [52]. As observed in Fig. 6(b), ΔG_H of p-WS_2 and srMoS_2 are ~0.35 and ~0.18 eV, respectively. Compared with p-WS_2, the Mo addition contributes to the decrease of ΔG_H, indicating that the formation of heterostructure is beneficial to improving the HER performances of tungsten disulfide. And when the W/Mo molar ratio is about 2:25, the value of ΔG_H is close to 0, reaching the minimum. With the further increase of Mo content, the corresponding ΔG_H is gradually enlarged, suggesting worse hydrogen desorption kinetics as well as HER activity, which is consistent with the experimental results.

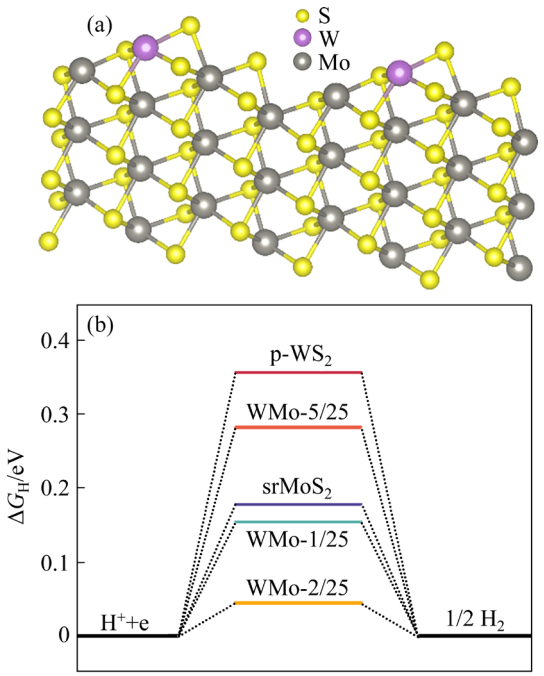

Fig. 6 Atomic structure model of WMo-2/25 (a), and Gibbs free energy diagrams of srMoS_2, p-WS_2 and MoS_2/WS_2 heterostructures with various proportions (b)

4 Conclusions

(1) With the presence of silica templates, the hollow heterostructures of MoS_2/WS_2 were successfully synthesized and adopted as HER electrocatalysts.

(2) The coexistence of petal-like MoS_2 and spherical shell-like WS_2 enables more active sites and better electron transfer ability.

(3) The DFT calculations reveal that the construction of MoS_2/WS_2 heterostructures with a W/Mo molar ratio of 2:25 leads to an optimized hydrogen adsorption energy, resulting in the best HER activity with a small Tafel slope of 53 mV/dec as well as excellent stability in acidic solution.

Acknowledgments

This work is supported from the Natural Science Foundation of Hunan Province of China (No. 2020JJ4730).

Supporting information

Supporting information in this paper can be found at: http://tnmsc.csu.edu.cn/download/18-p1540-2021-1526-supporting_information.pdf.

References

[1] AMORES E, SÁNCHEZ M, ROJAS N, SÁNCHEZ-MOLIN A M. Renewable hydrogen production by water electrolysis [M]//Sustainable Fuel Technologies Handbook. Amsterdam: Elsevier, 2021: 271−313.

[2] QURESHY A M M I Q, DINCER I. A new integrated renewable energy system for clean electricity and hydrogen fuel production [J]. International Journal of Hydrogen Energy, 2020, 45(41): 20944−20955.

[3] SUI Ji-yuan, CHEN Zhen-nan, WANG Chen, WANG Yue-yang, LIU Jian-hong, LI Wen-jia. Efficient hydrogen production from solar energy and fossil fuel via water-electrolysis and methane-steam-reforming hybridization [J]. Applied Energy, 2020, 276: 115409−115421.

[4] LAMICHANEY S, BARANWAL R, MAITRA S, MAJUMDAR G. Clean energy technologies: Hydrogen power and fuel cells [M]//Encyclopedia of Renewable and Sustainable Materials. Amsterdam: Elsevier, 2020: 366−371.

[5] YANG Fan, JIANG Liang-ing, YU Xiao-ying, LIU Fang-yang, LAI Yan-qing, LI Jie. Catalytic effects of NH_4^+ on hydrogen evolution and manganese electrodeposition on stainless steel [J]. Transactions of Nonferrous Metals Society of China, 2019, 29(11): 2430−2439.

[6] ZOU Xiao-xin, ZHANG Yu. Noble metal-free hydrogen evolution catalysts for water splitting [J]. Chemical Society Reviews, 2015, 44(15): 5148−5180.

[7] LIU Jiang-hua. Hydrogen energy—The green energy of the future [J]. Modern Chemical Industry, 2006, 26(2):10−15. (in Chinese)

[8] NG Kim-hoong, LAI Sin-yuan, CHENG Chin-kui, CHENG Yoke-wang, CHONG Chi-cheng. Photocatalytic water splitting for solving energy crisis: Myth, Fact or Busted? [J]. Chemical Engineering Journal, 2021, 417: 128847−128863.

[9] KIBSGAARD J, CHORKENDORFF I. Considerations for the scaling-up of water splitting catalysts [J]. Nature Energy, 2019, 4(6): 430−433.

[10] CHEN Yang-dong, ZHENG Ying, YUE Xin, HUANG Shao-ming. Hydrogen evolution reaction in full pH range on nickel doped tungsten carbide nanocubes as efficient and durable non-precious metal electrocatalysts [J]. International Journal of Hydrogen Energy, 2020, 45(15): 8695−8702.

[11] HAN Dong-chen, LUO Zhao-yan, LI Yang, GAO Nan-xing, GE Jun-jie, LIU Chang-peng, XING Wei. Synergistic engineering of MoS_2 via dual-metal doping strategy towards hydrogen evolution reaction [J]. Applied Surface Science, 2020, 529: 147117−147124.

[12] WANG Jia-jun, CHANG Kuan, SUN Ze-yu, LEE J H, BRIAN M T, ZHANG Cheng, CHEN Jing-guang, LIU Chang-jun. A Combined experimental and theoretical study of the accelerated hydrogen evolution kinetics over wide pH range on porous transition metal doped tungsten phosphide electrocatalysts [J]. Applied Catalysis B: Environmental, 2019, 251: 162−167.

[13] ZHANG Xiang-yong, LIU Tian-ying, GUO Ting, HAN Xue-ying, MU Zong-yun, CHEN Qiang, JIANG Jiang-min, YAN Jing, YUAN Jia-ren, WANG De-zhi, WU Zhuang-zhi, KOU Zong-kui. Controlling atomic phosphorous-mounting surfaces of ultrafine W_2C nanoislands monodispersed on the carbon frameworks for enhanced hydrogen evolution [J]. Chinese Journal of Catalysis, 2021, 42(10): 1798−1807.

[14] FEI Hao, GUO Ting, XIN Yue, WANG Liang-bing, LIU Ruo-qi, WANG De-zhi, LIU Fang-yang, WU Zhuang-zhi. Sulfur vacancy engineering of MoS_2 via phosphorus incorporation for improved electrocatalytic N_2 reduction to NH_3 [J], Applied Catalysis B: Environmental, 2022, 300: 120733.

[15] LIU Ruo-qi, GUO Ting, FEI Hao, WU Zhuang-zhi, WANG De-zhi, LIU Fang-yang. Highly efficient electrocatalytic N_2 reduction to ammonia over metallic 1T phase of MoS_2 enabled by active sites separation mechanism [J]. Advanced Science, 2022, 9(2): 2103583.

[16] KIM Seong-ku, SONG Wooseok, JI Seulgi, LIM Yi-rang, LEE Young-bum, MYUNG Sung, LIM Jong-sun, AN Ki-seok, LEE Sun-sook. Synergetic effect at the interfaces of solution processed MoS_2−WS_2 composite for hydrogen evolution reaction [J]. Applied Surface Science, 2017, 425: 241−245.

[17] CHEN Ya-qiong, ZHANG Jin-feng, WAN Lei, HU Wen-bin, LIU Lei, ZHONG Cheng, DENG Yi-da. Effect of nickel phosphide nanoparticles crystallization on hydrogen evolution reaction catalytic performance [J]. Transactions of Nonferrous Metals Society of China, 2017, 27(2): 369−376.

[18] THANGASAMY P, OH S, NAM S, OH I K. Rose-like MoS_2 nanostructures with a large interlayer spacing of ~9.9 Å and exfoliated WS_2 nanosheets supported on carbon nanotubes for hydrogen evolution reaction [J]. Carbon, 2020, 158: 216−225.

[19] GAO Tong, NIE Ming, LUO Jin, HUANG Zhi, SUN Hai, GUO Pei-tao, XUE Zhen-hong, LIAO Jian-ming, LI Qing, TENG Liu-mei. Nickel sulfides supported by carbon spheres as efficient catalysts for hydrogen evolution reaction [J]. Electrochemistry Communications, 2021, 129: 107076−107081.

[20] YUAN Tie-chui, LI Rui-di, ZHOU Ke-chao. Electrocatalytic properties of Ni−S−Co coating electrode for hydrogen evolution in alkaline medium [J]. Transactions of Nonferrous Metals Society of China, 2007, 17(4): 762−765.

[21] ZAHRA R, PERVAIZ E, YANG Ming-hui, RABI O, SALEEM Z, ALI M, FARRUKH S. A review on nickel cobalt sulphide and their hybrids: Earth abundant, pH stable electro-catalyst for hydrogen evolution reaction [J]. International Journal of Hydrogen Energy, 2020, 45(46): 24518−24543.

[22] WEI Qing-bo, YE Zhang-wen, REN Xian-pei, LI Xue, YIN Ming-li, ZAN Ling-xing, FU Feng. Core-shell CoS_2@MoS_2

nanoparticles as an efficient electrocatalyst for hydrogen evolution reaction [J]. Journal of Alloys and Compounds, 2020, 835: 155264−155280.

[23] CHEN Tzu-yin, CHANG Yung-huang, HSU Chang-lung, WEI Kung-hwa, CHIANG Chia-ying, LI Lain-jong. Comparative study on MoS_2 and WS_2 for electrocatalytic water splitting [J]. International Journal of Hydrogen Energy, 2013, 38(28): 12302−12309.

[24] GUO Zhuo, SUN Tian-shuai, LI Ya-hui, KANG Hai-lan, CHE Yu-han, ZHANG Yan, LU Jin-lin. Large surface and pore structure of mesoporous WS_2 and RGO nanosheets with small amount of Pt as a highly efficient electrocatalyst for hydrogen evolution [J]. International Journal of Hydrogen Energy, 2018, 43(51): 22905−22916.

[25] LONKAR S P, PILLAI V V, ALHASSAN S M. Three dimensional (3D) nanostructured assembly of MoS_2−WS_2/Graphene as high performance electrocatalysts [J]. International Journal of Hydrogen Energy, 2020, 45(17): 10475−10485.

[26] XU Xiang-fu, CHEN Jia, LAI Guo-xia, LI Tian-le, XU Shi-zhen, CHEN Xing-yuan, ZHU Wei-ling. Theoretical study on enhancing the monolayer MoS_2 photocatalytic water splitting with alloying and stress [J]. Journal of Fuel Chemistry and Technology, 2020, 48(3): 321−327.

[27] ZHANG Zheng, CHEN Kai, ZHAO Qiang, HUANG Mei, OUYANG Xiao-ping. Electrocatalytic and photocatalytic performance of noble metal doped monolayer MoS_2 in the hydrogen evolution reaction: A first principles study [J]. Nano Materials Science, 2021, 3(1): 89−94.

[28] CHEN Ya-jie, KANG Chuan-hong, WANG Rui-hong, REN Zhi-yu, FU Hui-ying, XIAO Yu-ting, TIAN Guo-hui. CoP/WS_2 nanoflake heterostructures as efficient electrocatalysts for significant improvement in hydrogen evolution activity [J]. Applied Surface Science, 2018, 442: 352−360.

[29] CAI Jian-nan, ZHANG Xiao-feng, PAN Yu-qi, KONG Yan-hong, LIN Shen. MoS_2||CoP heterostructure loaded on N, P-doped carbon as an efficient trifunctional catalyst for oxygen reduction, oxygen evolution, and hydrogen evolution reaction [J]. International Journal of Hydrogen Energy, 2021, 46(69): 34252−34263.

[30] LIU Qin, LI Xiu-ling, HE Qun, KHALIL A, LIU Dao-bin, XIANG Ting, WU Xiao-jun, SONG Li. Gram-scale aqueous synthesis of stable few-layered 1T-MoS_2: Applications for visible-light-driven photocatalytic hydrogen evolution [J]. Small, 2015, 11(41): 5556−5564.

[31] JAYABAL S, SARANYA G, LIU Yong-qiang, GENG Dong-sheng, MENG Xiang-bo. Unravelling synergy effects of defect-rich 1T-MoS_2/carbon nanotubes for the hydrogen evolution reaction by experimental and calculational studies [J]. Sustainable Energy & Fuels, 2019, 3(8): 2100−2110.

[32] NAYAK A P, PANDEY T, VOIRY D, LIU Jin, MORAN S T, SHARMA A, TAN Cheng, CHEN Chang-hsiao, LEE Lain-jong, CHHOWALLA M, LIN Jung-fu, SINGH A K, AKINWANDE D. Pressure-dependent optical and vibrational properties of monolayer molybdenum disulfide [J]. Nano Lett, 2015, 15(1): 346−353.

[33] LIU Shan-hu, XU Yin-xi, CHANDA D, TAN Lei, XING Rui-min, LI Xi-ying, MAO Li-qun, KAZUYA N, FUJISHIMA A. Ultrathin WS_2 nanosheets vertically aligned on TiO_2 nanobelts as efficient alkaline hydrogen evolution electrocatalyst [J]. International Journal of Hydrogen Energy, 2020, 45(3): 1697−1705.

[34] SONG Jeong-gyu, PARK Ju-sang, LEE Won-seon, CHOI Tae-jin, JUNG Hanearl, LEE Chang-wan, HWANG Sung-hwan, MYOUNG Jae-min, JUNG Jae-hoon, KIM Soo-hyun, CLEMENT L, KIM Hyung-jun. Layer-controlled, wafer-scale and conformal synthesis of tungsten disulfide nanosheets using atomic layer deposition [J]. ACS Nano, 2013, 7(12):11333−11340.

[35] SHANG Xiao, YAN Kai-li, LIU Zi-zhang, LU Shan-shan, DONG Bin, CHI Jing-qi, LI xiao, LIU Yan-ru, CHAI Yong-ming, LIU Chen-guang. Oxidized carbon fiber supported vertical WS_2 nanosheets arrays as efficient 3D nanostructure electrocatalyst for hydrogen evolution reaction [J]. Applied Surface Science, 2017, 402: 120−128.

[36] LIU Zheng-qing, LI Na, SU Cong, ZHAO Hong-yang, XU Ling-ling, YIN Zong-you, LI Ju, DU Ya-ping. Colloidal synthesis of 1T' phase dominated WS_2 towards endurable electrocatalysis [J]. Nano Energy, 2018, 50: 176−181.

[37] ZHAO Li-li, JIA Jin, YANG Zhi-yuan, YU Jia-yuan, WANG Ai-li, SANG Yuan-hua, ZHOU Wei-jia, LIU Hong. One-step synthesis of CdS nanoparticles/MoS_2 nanosheets heterostructure on porous molybdenum sheet for enhanced photocatalytic H_2 evolution [J]. Applied Catalysis B: Environmental, 2017, 210: 290−296.

[38] OSHIKAWA K, NAGAI M, OMI S. Characterization of molybdenum carbides for methane reforming by TPR, XRD, and XPS [J]. J Phys Chem B, 2001, 105: 9124−9131.

[39] ZHENG Guo-yuan, WU Cai-hong, WANG Ji-lin, MO Shu-yi, WANG Yan-wu, ZOU Zheng-guang, ZHOU Bing, LONG Fei. Facile synthesis of few-layer MoS_2 in MgAl-LDH layers for enhanced visible-light photocatalytic activity [J]. RSC Advances, 2019, 9(42): 24280−24290.

[40] ABINAYA R, ARCHANA J, HARISH S, NAVANEETHAN M, PONNUSAMY S, MUTHAMIZHCHELVAN C, SHIMOMURA M, HAYAKAWA Y. Ultrathin layered MoS_2 nanosheets with rich active sites for enhanced visible light photocatalytic activity [J]. RSC Advances, 2018, 8(47): 26664−26675.

[41] DANIEL E, NIU Yu-biao, PARK Sung-jin, MARK I, KAREN W, RICHARD E P, NEIL V R. Hydrogen evolution enhancement of ultra-low loading, size-selected molybdenum sulfide nanoclusters by sulfur enrichment [J]. Applied Catalysis B: Environmental, 2018, 235: 84−91.

[42] DONG Hai-feng, LIU Cong-hui, YE Hai-tao, HU Lin-ping, Bunshi F, DAI Wen-hao, CAO Yu, QI Xue-qiang, LU Hui-ting, ZHANG Xue-ji. Three-dimensional nitrogen-doped graphene supported molybdenum disulfide nanoparticles as an advanced catalyst for hydrogen evolution reaction [J]. Sci Rep, 2015, 5: 17542.

[43] WU Zhuang-zhi, FANG Bai-zeng, BONAKDARPOUR A, SUN Ao-kui, WILKINSON D P, WANG De-zhi. WS_2 nanosheets as a highly efficient electrocatalyst for hydrogen evolution reaction [J]. Applied Catalysis B: Environmental, 2012, 125: 59−66.

[44] SHENG W C, GASTEIGER H A, YANG S M. Hydrogen oxidation and evolution reaction kinetics on platinum: Acid vs alkaline electrolytes [J]. Journal of the Electrochemical

Society, 2010, 157(11): B1529−B1536.
[45] MERKI D, VRUBEL H, ROVELLI L, FIERRO S, HU Xi-le. Fe, Co, and Ni ions promote the catalytic activity of amorphous molybdenum sulfide films for hydrogen evolution [J]. Chemical Science, 2012, 3(8): 2515−2525.
[46] WANG Meng, MA Wan-sen, LV Ze-peng, LIU Dong, JIAN Kai-liang, DANG Jie. Co-doped Ni_3N nanosheets with electron redistribution as bifunctional electrocatalysts for efficient water splitting [J]. Journal of Physical Chemistry Letters, 2021, 12(6): 1581−1587.
[47] LV Ze-peng, MA Wan-sen, WANG Meng, DANG Jie, JIAN Kai-liang, LIU Dong, HUANG De-jun. Co-constructing interfaces of multiheterostructure on MXene ($Ti_3C_2T_x$)-modified 3D self-supporting electrode for ultraefficient electrocatalytic HER in alkaline media [J]. Advanced Functional Materials, 2021, 31(29): 2102576−2102584.
[48] LV Ze-peng, MA Wan-sen, DANG Jie, WANG Meng, JIAN Kai-liang, LIU Dong, HUANG De-jun. Induction of Co_2P growth on a MXene ($Ti_3C_2T_x$)-modified self-supporting electrode for efficient overall water splitting [J]. Journal of Physical Chemistry Letters, 2021, 12(20): 4841−4848.
[49] LV Ze-peng, WANG Meng, LIU Dong, JIAN Kai-liang, ZHANG Run, DANG Jie. Synergetic effect of Ni_2P and MXene enhances catalytic activity in the hydrogen evolution reaction [J]. Inorganic Chemistry, 2021, 60(3): 1604−1611.
[50] XIONG Kun, LI Li, ZHANG Li, DING Wei, PENG Li-shan, WANG Yao, CHEN Si-guo, TAN Shi-yu, WEI Zi-dong. Ni-doped Mo_2C nanowires supported on Ni foam as a binder-free electrode for enhancing the hydrogen evolution performance [J]. Journal of Materials Chemistry A, 2015, 3(5): 1863−1867.
[51] ANG Hui-xiang, WANG Huan-wen, LI Bing, ZONG Yun, WANG Xue-feng, YAN Qing-yu. 3D hierarchical porous Mo_2C for efficient hydrogen evolution [J]. Small, 2016, 12(21): 2859−2865.
[52] LI Hong-lin, YU Ke, TANG Zheng, ZHU Zi-qiang. Enhanced hydrogen evolution performance of ultra thin nanoslice/nanopetal structured XS_2 (X = W, Mo): From experiment to theory [J]. Journal of Applied Physics, 2016, 120(2): 024301−024310.

空心球壳状 MoS_2/WS_2 异质结构的制备及其电催化析氢性能

王德志，杨刘熠懿，刘若琦，郭 挺，费 浩，吴壮志

中南大学 材料科学与工程学院，长沙 410083

摘 要：系统研究一种由空心 WS_2 球壳和花瓣状 MoS_2 组成的异质结构。结果表明，空心球壳结构使活性位点更容易暴露，异质结构的形成有助于激发 WS_2 和 MoS_2 之间的协同效应，从而提高析氢反应性能，具有更好的电子转移能力。更重要的是，密度泛函理论计算进一步阐明了协同机理，表明 MoS_2/WS_2 异质结构可有效调节氢吸附自由能，使之在 W/Mo 原子比为 2:25 时达到最小值。因此，优化后的 WMo-2/25 催化剂表现出优异的电催化析氢活性，Tafel 斜率低，为 53 mV/dec，并具有良好的稳定性。

关键词：二硫化钼；二硫化钨；异质结构；析氢反应；密度泛函理论

(Edited by Xiang-qun LI)